

Raman polarization studies of highly oriented organic thin films

V. Presser,^a B.-E. Schuster,^{b*} M. B. Casu,^b U. Heinemeyer,^c F. Schreiber,^c K. G. Nickel^a and T. Chassé^b

In this work we report on the capability of polarized Raman spectroscopy to investigate the structure of thin organic films. Diindenoperylene (DIP) thin films on (1 × 1)-rutile(110) were prepared via organic molecular beam deposition (OMBD). Raman spectra of DIP thin films showed several strong Raman modes in the wavenumber region from 1200 to 1650 cm⁻¹. The A_g mode at 1284 cm⁻¹ shows two contributions, thereby indicating the coexistence of at least two DIP film structures. Polarized Raman spectroscopy was applied to characterize the molecular orientation and the dominance of the σ -configuration (i.e. upright standing DIP molecules) was found. Copyright © 2009 John Wiley & Sons, Ltd.

Keywords: diindenoperylene; polarized Raman spectroscopy; organic thin film; rutile; molecular orientation

Introduction

Organic materials play an increasingly important role in the field of electronic devices like field effect transistors or light emitting diodes. Two major advantages of organic semiconductors are their potential cost-efficiency when used in electronics or optoelectronics and their tunability by modifying specific functional groups.^[1–3] Organic molecules can be vapor-deposited under vacuum, spin-coated, dip-coated or printed on appropriate substrates depending on their solubility and behavior in solution. These techniques potentially reduce the problems related to growing or handling a single crystal and, not less important, they are crucial for low cost electronics. It is well-known that preparation parameters can significantly influence electronic properties, morphology, structure and molecular orientation of the organic thin film.^[4–7] Therefore, full characterizations of thin organic film structures are basic prerequisites for a comprehensive understanding, which eventually allows improving and tailoring of properties for widespread technical applications.

In this study we investigate thin films of diindenoperylene (DIP, C₃₂H₁₆) – a perylene-based polycyclic aromatic hydrocarbon – that has successfully been used to prepare thin films^[4,8] that show properties like high hole mobility^[9] and high thermal stability.^[10,11] Previous studies analyzed DIP thin films deposited on various substrate materials (e.g. sapphire, gold, rubrene) and two predominant ordering structures were described:^[4] (1) 'lying-down' (λ -configuration) and (2) 'standing-up' (σ -configuration) molecules. Recently, it has been shown that DIP films deposited on polycrystalline gold present flat lying molecules in the first layer, while the angle between the molecular axis and the surface increases with thickness.^[7] The choice of the substrate certainly influences the resulting structure of the organic thin film.^[4,5,9,11] We used for this study a well-known substrate material: rutile-phase titanium dioxide (TiO₂). Titanium dioxide, in general, is one of the most thoroughly investigated single-crystalline metal oxides^[12,13] and our choice was further motivated by the technical relevance of TiO₂ applications (e.g. in (photo)catalysis, optical coatings, photovoltaic cells).

In this work, we present Raman spectra of DIP on TiO₂(110) as a model system and use polarized Raman spectroscopy to show the potential of this technique applied to an organic thin film for identifying preferential molecular orientation.

Polarization-dependent Raman scattering is an established characterization method and it has proved to be a very powerful tool to investigate the domain orientation in inorganic polycrystalline materials.^[14–16] As for organic materials, it has successfully been applied for the study of single crystals and the molecular orientation of well-known polycrystalline thin films.^[17–19]

Analytical Methods

Substrate and film preparation

A clean rutile TiO₂(110) surface was prepared by a very gentle and brief Ar⁺ ion bombardment (500 V), followed by annealing in ultra high vacuum (UHV) at approximately 830 K. This procedure has proved to be a suitable preparation method for rutile(110) single crystals.^[20] We obtained a sharp (1 × 1) reconstruction low energy electron diffraction (LEED) pattern. The Ti2p photoemission spectrum showed only a very weak high kinetic energy shoulder that is most commonly attributed to the presence of surface non-stoichiometry due to oxygen vacancies.

* Correspondence to: B.-E. Schuster, Institute for Physical and Theoretical Chemistry, University of Tübingen, Auf der Morgenstelle 8, D-72076 Tübingen, Germany. E-mail: britt.schuster@uni-tuebingen.de

^a Institute for Geoscience, Applied Mineralogy, University of Tübingen, Wilhelmstraße 56, D-72074 Tübingen, Germany

^b Institute for Physical and Theoretical Chemistry, University of Tübingen, Auf der Morgenstelle 8, D-72076 Tübingen, Germany

^c Institute for Applied Physics, University of Tübingen, Auf der Morgenstelle 10, D-72076 Tübingen, Germany

Thin films of DIP were prepared by organic molecular beam deposition (OMBD) *in situ* using strictly controlled evaporation conditions (evaporation rate of 3 Å/min and substrate temperature of 298 K). Thin film growth was monitored using a quartz crystal microbalance. A nominal film thickness of 7 nm was measured after deposition.

Substrate and film characterization

Raman scattering measurements were performed in back-scattering geometry using a confocal Raman spectrometer (Dilor Labram[®] 2; now Horiba Jobin Yvon, Bensheim, Germany) equipped with a 1800 lines/mm grating and an external argon ion laser (488 nm). The laser beam was focused onto the sample by a 50-fold magnifying microscope objective (numeric aperture $NA = 0.55$) leading to a laser beam of approximately 1 μm in diameter. The spectral resolution was about 1.7 cm⁻¹. In order to prevent radiation damage, a laser power ≤ 1 mW was used and the measurement times were in the range of tens of seconds. For more details on the lateral, axial and spectral resolution of this spectrometer see Ref. [21].

For polarized Raman studies we employed two different measuring procedures: (1) a fixed setup for the polarizer and analyzer, rotating the sample (sample rotation angle δ) and (2) a fixed analyzer and sample position, varying the polarization direction of the incident light (polarization direction rotation angle γ).

For the first setup, we performed measurements both in parallel and in cross polarization configurations. These results may be directly compared with other studies on polarized Raman spectroscopy, because most of them follow this approach. The error of angle determination in the rotation of the sample around its surface normal was about ±3°.

Rotation of the polarization direction by inserting a lambda-half-plate (second setup) ensured that the very same sample position could be probed. On the contrary, the rotation of the sample causes a different area to be examined with our apparatus, because optical and rotational axes do not coincide ideally. The polarization direction was adjustable within ±1° by use of a computer controlled stepping motor.

For both setups, on rotating either the polarization direction or the sample itself while leaving the analyzer direction unchanged, grating characteristics (i.e. intensity change due to angle-dependent reflectivity) did not have to be corrected for. The intensity reproducibility of the Raman signal was approximately ±8%.

Spectra analysis was performed using commercially available software (Origin 7.5, OriginLab Corporation, Northampton, U.S.A.; Labspec 4.02, Horiba Jobin Yvon, Bensheim, Germany). Raman intensities were evaluated after subtracting a linear base line and fitting a Voigt profile.^[22]

Results and Discussion

Determination of the crystallographic axes of the rutile substrate

Before characterizing the thin films, we performed polarized Raman spectroscopy in order to determine the exact orientation of the crystallographic axes of rutile(110). *A priori*, only the direction of the z-axis ([001] = perpendicular to the surface normal) was known from the crystallographic cut of the single crystal.

Rutile is tetragonal (space group $D^{14}_{4h} = P4_2/mnm$) with two TiO₂ units per unit cell. Of the 11 vibrational modes with the irreducible representation $A_{1g} + A_{2g} + A_{2u} + B_{1g} + B_{2g} + 2B_{1u} + E_g + 3E_u$ expected, four of the modes [A_{1g} (612 cm⁻¹), B_{1g} (143 cm⁻¹), B_{2g} (826 cm⁻¹) and E_g (447 cm⁻¹)] are Raman active^[23] and four modes are infrared active ($A_{2u} + 3E_u$). We chose the rutile A_{1g} and E_g modes to determine the crystal orientation.

In general, the intensity of Raman bands can be expressed as a function of crystal orientation and polarization geometry^[16,24] according to Eqn (1):

$$I \propto |e_i \cdot \mathfrak{R} \cdot e_s|^2 \quad (1)$$

where I is the reflected Raman intensity, e_i and e_s are the unit polarization vectors of the electric field for the incident (e_i) and the scattered (e_s) laser beams, respectively, and \mathfrak{R} represents the Raman scattering tensor of a specific vibrational mode. In the case of rutile, Raman tensors of the A_{1g} and E_g modes have the following overall form^[23,25] (Eqn (2)):

$$\mathfrak{R}(A_{1g}) = \begin{bmatrix} a & 0 & 0 \\ 0 & a & 0 \\ 0 & 0 & b \end{bmatrix}; \mathfrak{R}(E_g) = \begin{bmatrix} 0 & 0 & 0 \\ 0 & 0 & d \\ 0 & d & 0 \end{bmatrix}, \begin{bmatrix} 0 & 0 & d \\ 0 & 0 & 0 \\ d & 0 & 0 \end{bmatrix} \quad (2)$$

The laboratory (reference) coordinate system was chosen in such a manner that the $[1\bar{1}0]$ direction of the crystal coincides with the x-axis of the reference system, while the $[001]$ direction of the crystal is parallel to the z-axis (i.e. $x = [1\bar{1}0]$, $y = [110]$ and $z = [001]$). Figure 1 shows the polarization dependence of the A_{1g} (612 cm⁻¹) and E_g (447 cm⁻¹) modes of rutile TiO₂(110). On probing different polarization configurations [Fig. 1a–d: $y(xx)\bar{y}$, $y(xz)\bar{y}$, $y(zx)\bar{y}$ and $y(zz)\bar{y}$] and, thereby different Raman scattering tensors components, the relative intensities of the A_{1g} mode (612 cm⁻¹) and E_g mode (447 cm⁻¹) greatly change,^[23] indicating the crystal orientation.

Rotating the sample allowed us to study the angle-dependence of the measured Raman intensity (Fig. 2a) of A_{1g} and E_g -modes. Using a parallel polarization configuration [$y(xx)\bar{y}$], we calculated the theoretical angular-dependent Raman intensity for the A_{1g} -mode at 612 cm⁻¹ by using Eqns (1) and (2) resulting in Eqn (3):

$$I \propto |a \cdot \cos^2 \delta + b \cdot \sin^2 \delta|^2 \quad (3)$$

where a and b denote Raman tensor components of the A_{1g} mode (612 cm⁻¹) and δ denotes the rotation angle around the surface normal. The experimental data of the A_{1g} -mode intensity agrees very well with the theoretical angular-dependency according to Eqn (3) (Fig. 2b).

Raman spectrum of diindenoperylene

In Fig. 3, a typical Raman spectrum of DIP (powder sample) is shown where a strong luminescence background (fluorescence) superimposes the Raman scattering. Using 488.0 nm as exciting wavelength, the spectrum is resonant.^[26,27] The most intensive Raman modes occur in the higher wavenumber region (1200–1650 cm⁻¹).

No experimental Raman spectra of DIP have been reported so far, but theoretical calculations (Ref. [28]), concerned mainly with the vibronic coupling constants, show that the breathing modes affect mainly the perylene core and are therefore similar to 3,4,9,10-perylene-tetracarboxylic-dianhydride (PTCDA). For that reason, we

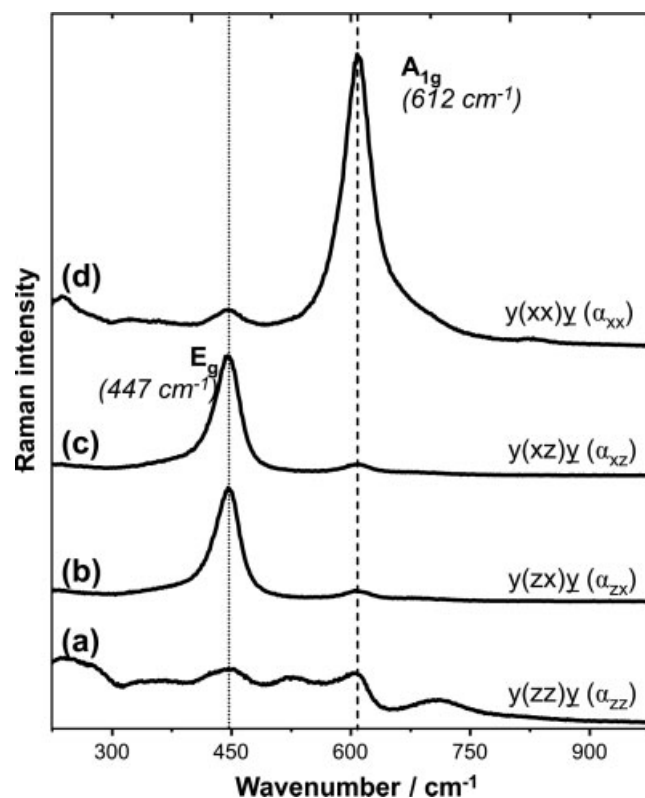


Figure 1. Polarized Raman spectra of rutile $\text{TiO}_2(110)$. Different polarization configurations (a–d) yield Raman spectra that are in agreement with the determined crystal orientation and with the literature (Ref. [23]). α_{ij} denotes the probed Raman tensor component. For discussion see text.

use Raman data of the perylene-based molecule PTCDA^[17,29–31] to assign the prominent vibrational modes of the DIP Raman spectrum.

The most prominent mode at 1284 cm^{-1} can be assigned to a symmetrical C–H in-plane bending mode (A_g).^[17,29,30] Since this vibrational mode is the strongest in the Raman spectrum, we used this mode to investigate the molecular orientation within the thin DIP film. The lowest Raman-active internal vibrational mode of the PTCDA molecule is located at 233 cm^{-1} .^[29] In analogy, DIP shows a Raman mode at 220 cm^{-1} that can be assigned to a breathing vibration of the molecule. The Raman mode at 1611 cm^{-1} can be assigned to C=C stretching vibrations.

According to both Tenne *et al.*^[29] and Zahn *et al.*^[17] almost every Raman mode of PTCDA in the wavenumber region $200\text{--}1700\text{ cm}^{-1}$ is assigned to an A_g mode. Therefore, in analogy, most Raman modes of DIP occurring between 200 and 1700 cm^{-1} may be assigned to A_g symmetry.

The structure of the DIP molecule is shown in Fig. 3. Assuming a planar geometry, D_{2h} is the point group of the free molecule. In the case of crystalline solid state samples, the site group and the factor group have to be considered, too. However, we will not consider these solid state effects because the aim of this paper is to show how it is possible to gain information about the thin film structure and the molecular orientation by using polarization-dependent Raman spectroscopy, starting with a minimal set of information, namely the point group of the free molecule and its position with respect the laboratory system.

Polarized Raman scattering of DIP thin film on (1×1) -rutile(110)

Contributions to the C–H bending mode in the context of different DIP thin film structures

Figure 4 shows a Raman spectrum of DIP on rutile(110) collected for both crossed and parallel polarization configuration – that is $y(xz)\bar{y}$ and $y(zz)\bar{y}$. The Raman modes of DIP in the lower wavenumber region ($200\text{--}800\text{ cm}^{-1}$) are superimposed by intense Raman modes of the rutile(110) substrate and therefore will not be used for the interpretation of the polarization measurements. Closer examination of the in-plane C–H bending mode at 1284 cm^{-1} (inset in Fig. 4) evidences a high-wavenumber shoulder. Profile line deconvolution yields two Raman bands located at $1284 \pm 0.2\text{ cm}^{-1}$ and $1289 \pm 0.5\text{ cm}^{-1}$, respectively.

Besides the static correlation field splitting, the Raman spectrum of organic crystals may differ from Raman spectra of the free molecule because of the dynamic correlation field splitting (Davydov splitting).^[32] Because of coupling of vibrations of different molecules in a unit cell, each internal molecular vibration mode splits into a multiplet, whereas the energetic separation between the vibrational levels depends on the strength of the intermolecular interaction (dipole and quadrupole interaction) within the unit cell.^[33] In the case of PTCDA crystals it is reported that the C–H bending mode exhibits a Davydov-splitting of 1.7 cm^{-1} and the other modes in the higher wavenumber region ($1200\text{--}1600\text{ cm}^{-1}$) show a splitting ranging from 0.7 to 2.4 cm^{-1} .^[29] Therefore, the 5 cm^{-1} wavenumber shift of the DIP C–H bending mode at 1284 cm^{-1} is possibly far too large for a Davydov splitting.

Theoretical calculations showed that small changes in the molecular environment can lead to significant wavenumber shifts for modes with pure C–H deformation character.^[17] Therefore, another explanation for the two band contributions is the presence of two different DIP phases, which may represent different crystallographic modifications or different molecular environments within the thin film.

Salvan^[34] and Das *et al.*^[35] reported for thin films of PTCDA a 3.8 cm^{-1} splitting of the C–H bending mode (located at 1303 cm^{-1}) as a result of the coexistence of different film structures (i.e. α - and β -polymorphs), where the lower wavenumber mode was assigned to molecules that experience a denser molecular packing.

Near edge X-ray absorption fine structure (NEXAFS) measurements^[36] of at least 2 nm thick DIP films on rutile(110) or of nominally thick DIP films (2 nm or thicker) on rutile(110) reveal a strong tendency toward upright standing DIP molecules (σ -configuration). In particular, we found an inclination angle $50^\circ < \Phi < 90^\circ$ between the molecular and the substrate planes. In contrast to this, NEXAFS spectra taken from thin DIP films ($<7\text{ \AA}$) do not show a strong dichroism (i.e. not a pronounced orientation). Therefore, statistically oriented small crystallites or disordered molecules may be present in these thin films, which may be influenced by the presence of substrate defects.

As a consequence, the polarized Raman spectra also reflect the coexistence of (at least) two different molecular orientations for the DIP thin films: (1) a rather disordered configuration in the form of statistically orientated nanoscale domains, and (2) the upright standing σ -orientation. Both configurations may well cause different molecular packing environments, resulting in different strengths of intermolecular forces (e.g. hydrogen bridges) which, finally, give rise to the observed band contributions. The

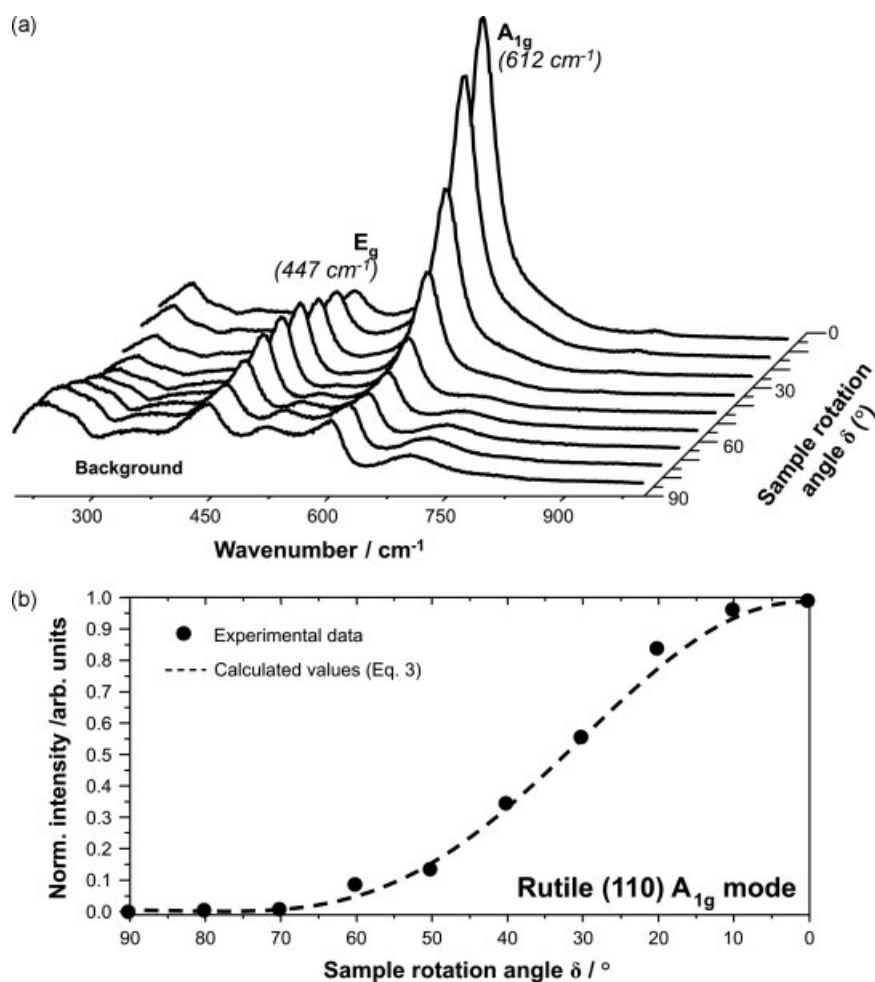


Figure 2. (a) Angle-dependent Raman spectra of rutile(110): Raman spectra of rutile TiO₂(110) upon rotation of the sample around its surface normal ($y(xx)\bar{y}$). (b) Angle-dependent Raman intensity of A_{1g} mode of rutile(110): Raman intensity change of the A_{1g} mode (612 cm⁻¹) upon sample rotation δ . The experimental data can be fitted excellently by use of Eqn (3).

small high-wavenumber shoulder may therefore be interpreted as being associated with the disordered DIP configuration (i.e. less dense molecular packing).

However, since in the present system there is also a significant inhomogeneity due to different crystal structures/orientations, it is difficult to draw a definitive conclusion on this. Calculations with density functional theory are presently performed to further clarify these findings.

Polarized Raman Spectroscopy and Preferential Orientation

In order to characterize the actual molecular orientation in thin DIP films by means of polarized Raman spectroscopy, the angular dependence of the DIP A_g mode at 1284 cm⁻¹ was studied. Figure 5 depicts the angular intensity dependency upon rotation of the polarization direction. The sample is aligned so that the parallel polarization configuration in Fig. 5a [$\gamma = 0^\circ$: $y(xx)\bar{y}$] and Fig. 5b [$\gamma = 0^\circ$: $y(zz)\bar{y}$] is parallel to the $[1\bar{1}0]$ and $[001]$ directions of the rutile crystal, respectively.

Periodic variations ($0 < \gamma < \pi$) of the intensity of the A_g mode of DIP at 1284 cm⁻¹ are clearly visible. The band at 1284 cm⁻¹ was fitted by profile line deconvolution excluding the shoulder at

1289 cm⁻¹. The latter showed a poor angular dependency, which is reasonable in the context of its attribution to a disordered DIP configuration.

The A_g mode of DIP shows an intensity minimum for the $y(xx)\bar{y}$ configuration, where the sampling direction coincides with the $[1\bar{1}0]$ direction of the rutile(110) crystal (Fig. 5a), whereas it exhibits a maximum in absolute intensity (Fig. 5b) after 90° rotation of the rutile substrate, i.e. on measuring along the $[001]$ direction of rutile. When evaluating the angular intensity dependency of the DIP A_g mode at 1284 cm⁻¹ it is important to note that the intensity change (minimum vs maximum) is about one order of magnitude higher for the configuration in Fig. 5b than for the one in Fig. 5a. This behavior is consistent with the results obtained with the second experimental approach, in which the rotation of the sample is carried out using a fixed polarizer/analyzer configuration (Fig. 6).

Figure 6 shows the angular dependence of the A_g mode of DIP (1284 cm⁻¹) and some Raman modes of rutile(110) for crossed (Fig. 6a) and parallel (Fig. 6b) polarization configurations. The sample was rotated clockwise azimuthally in steps of 10° and the measured Raman intensity of the A_g mode varied with periods of 180 and 90° in parallel and in crossed polarization configurations, respectively. The maximum response in parallel polarization for the A_g modes is observed for both setups, rotating either the sample

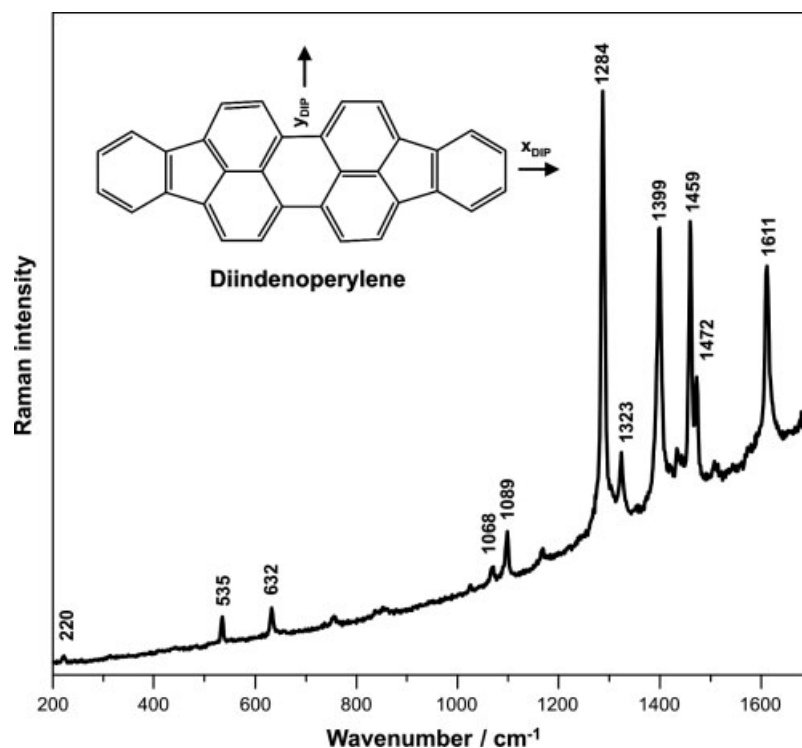


Figure 3. Raman spectrum of diindenoperylene (DIP) powder and molecular structure of DIP (inset). For discussion see text.

or the polarization direction, when the electric field vectors are parallel to the [001] direction of the substrate.

The clear angular dependency of the Raman signal evidences a preferential molecular orientation within the DIP thin film. If the DIP molecules were statistically distributed within the probed volume of the thin film, such distinct angular dependent Raman intensity would not be observed.

For the free DIP molecule, the D_{2h} point group has to be considered. Thus, the Raman tensor for A_g has the form (Eqn (4), Refs [25,37]):

$$\mathfrak{R}(A_g) = \begin{bmatrix} a & 0 & 0 \\ 0 & b & 0 \\ 0 & 0 & c \end{bmatrix} \quad (4)$$

First, we consider the DIP molecule to be present in the lying down λ -configuration with no azimuthal distribution. Even though we do not know the value of the individual Raman tensor components, the scattered A_g mode intensity would completely vanish when rotating the sample under crossed poles condition at a certain rotation angle. However, all A_g modes had a significant residual intensity for all sample rotation angles under crossed poles condition. This can only be explained when the molecules are not perfectly azimuthally ordered. The same applies for the σ -configuration.

In case of a perfectly azimuthally ordered λ -configuration above a highly disordered DIP configuration, the measured residual Raman intensity would show an increased signal from the 1289 cm^{-1} band which, in fact, cannot be observed (*cf* Fig. 4).

We now consider the three molecular axes x_{DIP} , y_{DIP} and z_{DIP} for a flat lying molecule using the Euler angles φ , θ and ψ to define

modified Raman tensors after rotation (Eqns (5)–(7)).

$$\mathfrak{R}_{(A_g)}^{x_{\text{DIP}}} = \begin{bmatrix} a & 0 & 0 \\ 0 & b \cdot \cos^2 \varphi + c \cdot \sin^2 \varphi & 0 \\ 0 & b \cdot \cos \varphi \cdot \sin \varphi - c \cdot \cos \varphi \cdot \sin \varphi & 0 \\ 0 & b \cdot \cos \varphi \cdot \sin \varphi - c \cdot \cos \varphi \cdot \sin \varphi & 0 \\ 0 & c \cdot \cos^2 \varphi + b \cdot \sin^2 \varphi & 0 \end{bmatrix} \quad (5)$$

$$\mathfrak{R}_{(A_g)}^{y_{\text{DIP}}} = \begin{bmatrix} a \cdot \cos^2 \theta + c \cdot \sin^2 \theta & 0 & 0 \\ 0 & b & 0 \\ a \cdot \cos \theta \cdot \sin \theta - c \cdot \cos \theta \cdot \sin \theta & 0 & 0 \\ a \cdot \cos \theta \cdot \sin \theta - c \cdot \cos \theta \cdot \sin \theta & 0 & 0 \\ 0 & 0 & 0 \\ c \cdot \cos^2 \theta + a \cdot \sin^2 \theta & 0 & 0 \end{bmatrix} \quad (6)$$

$$\mathfrak{R}_{(A_g)}^{z_{\text{DIP}}} = \begin{bmatrix} a \cdot \cos^2 \psi + b \cdot \sin^2 \psi & 0 & 0 \\ a \cdot \cos \psi \cdot \sin \psi - b \cdot \cos \psi \cdot \sin \psi & 0 & 0 \\ 0 & 0 & 0 \\ a \cdot \cos \psi \cdot \sin \psi - b \cdot \cos \psi \cdot \sin \psi & 0 & 0 \\ b \cdot \cos^2 \psi + a \cdot \sin^2 \psi & 0 & 0 \\ 0 & 0 & c \end{bmatrix} \quad (7)$$

For the higher-symmetrical copper phthalocyanine molecule (CuPc, Ref. [19]), $a = b$ and $x_{\text{CuPc}} = y_{\text{CuPc}}$. Therefore, Basova and Kolesov^[19] were able to calculate molecular plane inclination angles directly from a constant value of the depolarization ratio under the assumption $c = 0$. In our case, we do not know the ratios among the tensor components a , b and c .

For an approximation of the molecular orientation, we performed a least-square-fit on the experimental data using a Levenberg-Marquard algorithm. In particular, we used the data presented in Fig. 5 (rotation of the polarization direction only),

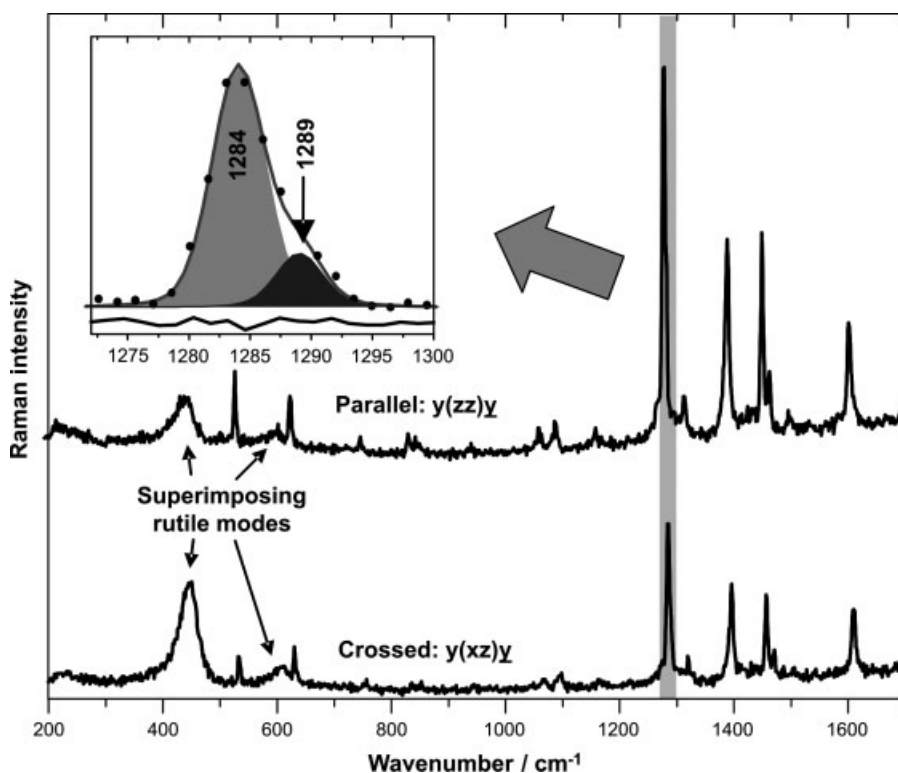


Figure 4. Raman spectra of DIP on rutile(110) in parallel $y(zz)y$ and crossed polarization $y(xz)y$ configurations. The insert shows that the A_g mode of DIP at $\approx 1284\text{ cm}^{-1}$ is actually composed of two individual Raman-active bands; the band positions were determined using profile line deconvolution and the residual for the peak fit is shown. For discussion see text.

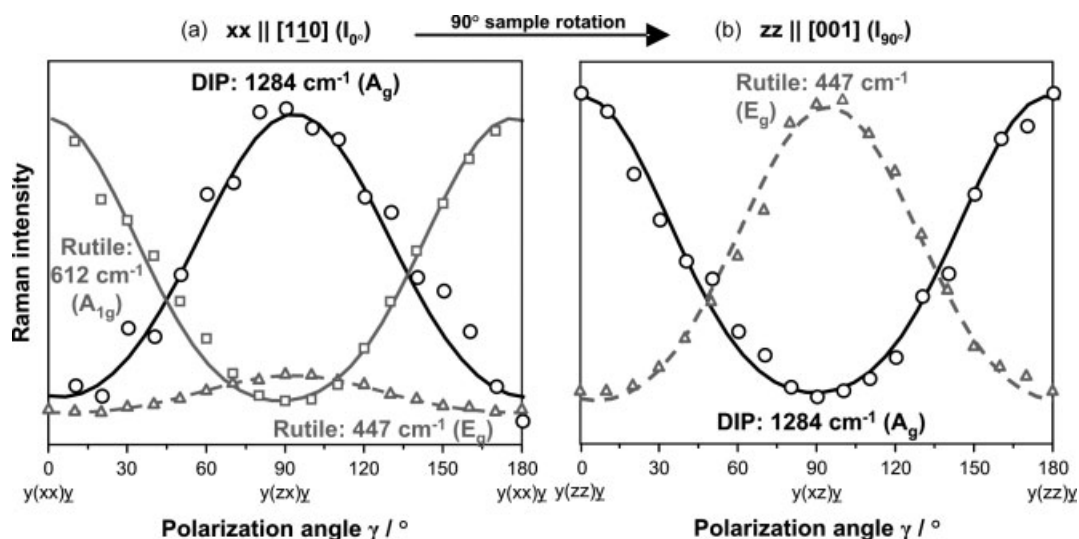


Figure 5. Polarization dependence of the A_g (1284 cm^{-1}) mode of DIP on rutile(110) for two different sample alignments: The sample is aligned so that the parallel polarization configuration in (a) and (b) is parallel to the $[1\bar{1}0]$ and $[001]$ directions of the crystal, respectively. For the purpose of comparison intensity changes of Raman modes (A_{1g} and E_g) from rutile(110) are included.

where the intensity for the first fixed sample orientation (I_{0°) is divided by the second set of data (i.e. after 90° rotation of the sample = I_{90°). For the refinement, we used the Euler angles φ , θ and ψ as variables. The transformed Raman tensor can be expressed as (Eqn (8)):

$$\mathfrak{R}_{(A_g)}^{\varphi\theta\psi} = \mathfrak{R}_{(A_g)}^\varphi \cdot \mathfrak{R}_{(A_g)}^\theta \cdot \mathfrak{R}_{(A_g)}^\psi \quad (8)$$

Also, we consider the rotation of the polarization direction γ (Eqns (9) and (10)):

$$e_i^{0^\circ} = (\sin(\gamma) \quad 0 \quad \cos(\gamma)) \quad (9)$$

$$e_i^{90^\circ} = (\cos(\gamma) \quad 0 \quad \sin(\gamma)) \quad (10)$$

We started for the 0° experiment with probing the α_{xx} -component and for the 90° experiment the α_{zz} -component. As the

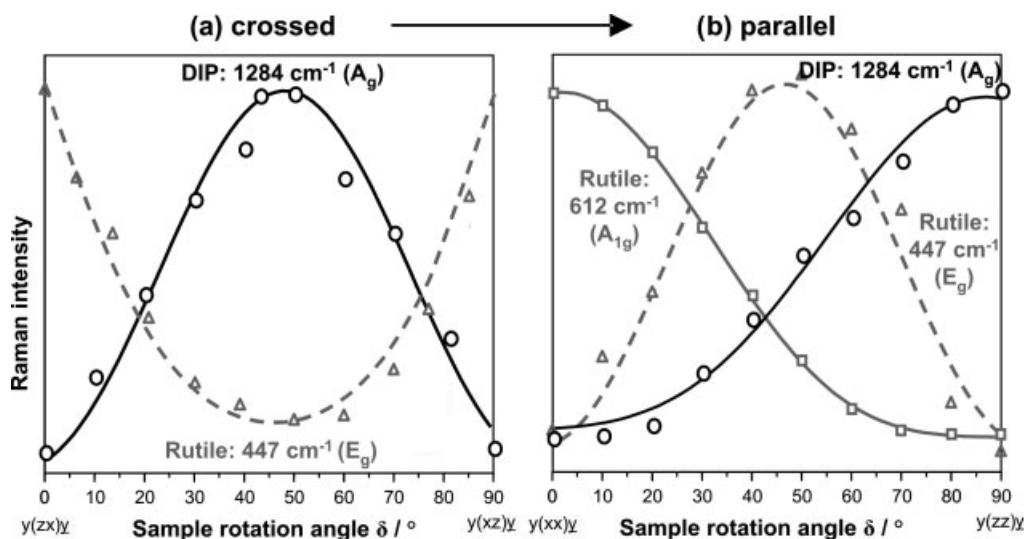


Figure 6. Intensity change of Raman scattering signals of the A_g mode of DIP (1284 cm^{-1}) and A_g (612 cm^{-1}) and E_g (450 cm^{-1}) of rutile(110) upon sample rotation around its surface normal. A clear angle dependence of the A_g modes of DIP for cross (a) and parallel (b) polarization conditions is visible.

sample, not the analyzer, is rotated by 90° , the analyzer is parallel to the z-axis of the rutile crystal for the 90° experiment (Eqns (11) and (12)).

$$e_s^{0^\circ} = \begin{pmatrix} 1 \\ 0 \\ 0 \end{pmatrix} \quad (11)$$

$$e_i^{90^\circ} = \begin{pmatrix} 0 \\ 0 \\ 1 \end{pmatrix} \quad (12)$$

The intensity ratio (I_{0°/I_{90°) can be calculated using Eqn (13):

$$\vartheta = \frac{I_{0^\circ}}{I_{90^\circ}} = \frac{|e_i^{0^\circ} \cdot \mathfrak{N}_{(A_g)}^{\varphi\theta\psi} \cdot e_s^{0^\circ}|^2}{|e_i^{90^\circ} \cdot [\mathfrak{N}_{(A_g)}^{z=90^\circ} \cdot \mathfrak{N}_{(A_g)}^{\varphi\theta\psi} \cdot \mathfrak{N}_{(A_g)}^{z=90^\circ}] \cdot e_s^{90^\circ}|^2} \quad (13)$$

To compensate for an angular spread of the collected beam, non-uniform thickness and surface roughness, Eqn (13) was modified (Refs [34,38,39]):

$$\vartheta_{\text{mod}} = \frac{(1 - \varepsilon) \cdot I_{0^\circ} + \varepsilon \cdot I_{90^\circ}}{\varepsilon \cdot I_{0^\circ} + (1 - \varepsilon) \cdot I_{90^\circ}} \quad (14)$$

For the fit we followed the same approach as that of Salvan^[34] and Kolesov *et al.*,^[18] with $a > b$ ($a = 1; b = 0.04$), $c = 0$. Figure 7 shows the experimental data for I_{0°/I_{90° and the calculated angular dependency using Eqn (14). Thus, we obtained the Euler angles $\varphi = 5^\circ \pm 7^\circ$, $\theta = 89^\circ \pm 5^\circ$ and $\psi = 0^\circ \pm 8^\circ$ which mean that (1) the effective molecular plane of this rather complex structure is tilted with respect to the substrate plane (110) by $89^\circ \pm 5^\circ$, (2) the molecules extend out of the substrate plane with their long axes (σ -configuration) and (3) the molecules are well-aligned to each other and adopt an orientation having their molecular planes parallel to the [001] direction of the substrate.

This is in agreement with the angular intensity dependency of the depolarization ratio. However, because of the uncertainties the real errors of the calculated values may be larger and also the resonant Raman process can introduce additional complications.

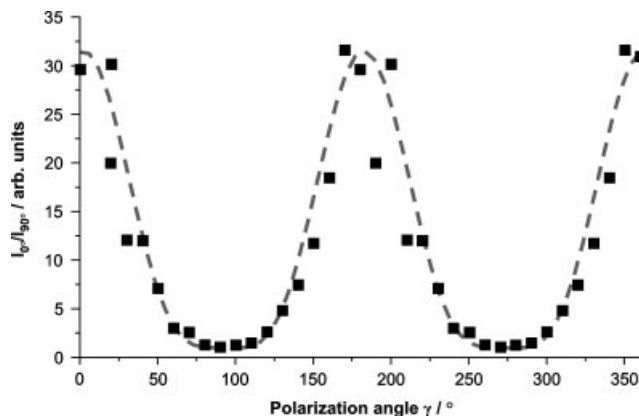


Figure 7. Measured (filled squares) and calculated (dotted line) values for the I_{0°/I_{90° intensity ratio. The fit yielded for $a = 1$, $b = 0.04$, $c = 0$ (a , b , $c = \text{fix}$) the Euler angles $\varphi = 5^\circ \pm 7^\circ$, $\theta = 89^\circ \pm 5^\circ$ and $\psi = 0^\circ \pm 8^\circ$ ($R^2 = 0.91$).

The least-square-fit yielded a very small ε value ($\varepsilon < 0.1$). The parameter ε is a factor depending on angular spread and surface imperfections, and when small, it indicates the presence of a highly ordered thin film structure.

The same angular dependency of polarized DIP Raman scattering in relation to the rutile substrate was observed on the whole DIP thin film. This means that the same effective molecular orientation characterizes the entire film.

Conclusions

In conclusion we have shown that polarization dependent Raman spectroscopy is an interesting tool for studying highly oriented organic thin films. As a model system we have chosen DIP films on rutile $\text{TiO}_2(110)$. It was shown that (1) the films are characterized by highly orientation order (clear angular dependence of the Raman signal), (2) they show at least two different structures (two contributions to the C–H bending mode located at 1284 and 1289 cm^{-1} , respectively) and (3) the molecules assume an up-right

standing position with respect to the substrate (least-square-fit of the experimental data).

Even organic thin films (≈ 7 nm nominal scale thickness), which are notoriously sensitive to radiation damage, could be investigated for their preferential molecular orientation. With measurement times in the range of several seconds or minutes, information on the preferential orientation of DIP thin films can be gained in a fast way. There are, however, still limitations to the calculation of the exact molecular orientation.

Certainly, polarized Raman spectroscopy cannot replace detailed synchrotron experiments. But at the very least, fast Raman mappings of large sample areas can be used to pre-characterize samples. Especially for systematic studies of the organic thin film growth Raman spectroscopy may become the method of choice.

Acknowledgements

Funding by the Ministerium für Wissenschaft, Forschung und Kunst FSP Baden-Württemberg, AZ 24-7532.23-21-18/2 is gratefully acknowledged. The authors thank Dr Francesco Allegretti, University of Graz, and Dr Reinhard Scholz, Technical University of Munich, respectively, for helpful discussions on rutile(110) surface preparation and Raman spectroscopy. Also, the authors wish to express their gratitude to the workshop of the Institute of Geoscience for carrying out necessary modifications of the Raman spectrometer.

References

- [1] R. H. Friend, R. W. Gymer, A. B. Holmes, J. H. Burroughes, R. N. Marks, C. Taliani, D. D. C. Bradley, D. A. Dos Santos, J. L. Bredas, M. Logdlund, W. R. Salaneck, *Nature* **1997**, *397*, 121.
- [2] G. Horowitz, *Adv. Mater.* **1998**, *10*, 365.
- [3] J. R. Sheats, *J. Mater. Res.* **2004**, *19*, 1974.
- [4] S. Kowarik, A. Gerlach, S. Sellner, F. Schreiber, L. Cavalcanti, O. Konovalov, *Phys. Rev. Lett.* **2006**, *96*, 125504/1.
- [5] S. Kowarik, A. Gerlach, F. Schreiber, *J. Phys.: Condens. Matter* **2008**, *20*, 184005/1.
- [6] S. Kera, M. B. Casu, K. R. Bauchspiess, D. Batchelor, T. Schmidt, E. Umbach, *Surf. Sci.* **2006**, *600*, 1077.
- [7] M. B. Casu, I. Biswas, B.-E. Schuster, M. Nagel, P. Nagel, S. Schuppler, T. Chassé, *Appl. Phys. Lett.* **2008**, *93*, 024103/1.
- [8] A. C. Dürr, F. Schreiber, M. Münch, N. Karl, B. Krause, V. Kruppa, H. Dosch, *Appl. Phys. Lett.* **2002**, *81*, 2276.
- [9] N. Karl, *Synth. Met.* **2003**, *133–134*, 649.
- [10] S. Sellner, A. Gerlach, F. Schreiber, M. Kelsch, N. Kasper, H. Dosch, S. Meyer, J. Pflaum, M. Fischer, B. Gompf, *Adv. Mater.* **2004**, *16*, 1750.
- [11] A. C. Dürr, F. Schreiber, M. Kelsch, H. D. Carstanjen, H. Dosch, *Adv. Mater.* **2002**, *14*, 961.
- [12] U. Diebold, *Appl. Phys. A* **2003**, *76*, 681.
- [13] U. Diebold, *Surf. Sci. Rep.* **2003**, *48*, 53.
- [14] M. Deluca, T. Sakashita, W. Zhu, H. Chazono, G. Pezzotti, *J. Appl. Phys.* **2007**, *101*, 083526-1–083526-3.
- [15] M. Deluca, T. Sakashita, G. Pezzotti, *Appl. Phys. Lett.* **2007**, *90*, 051919-1–051919-3.
- [16] M. S. Amer, J. Maguire, L. Cai, R. Biggers, J. Busbee, S. R. LeClair, *J. Appl. Phys.* **2001**, *89*, 8030.
- [17] D. R. T. Zahn, G. N. Gavrila, G. Salvan, *Chem. Rev.* **2007**, *107*, 1161.
- [18] B. A. Kolesov, T. V. Basova, I. K. Igumenov, *Thin Solid Films* **1997**, *304*, 166.
- [19] T. V. Basova, B. A. Kolesov, *Thin Solid Films* **1998**, *325*, 140.
- [20] F. Allegretti, S. O'Brien, M. Polcik, D. I. Sayago, D. P. Woodruff, *Phys. Rev. Lett.* **2005**, *95*, 226104/1.
- [21] V. Presser, C. Glotzbach, *J. Raman Spectrosc.* **2009**, *40*, 491.
- [22] V. Presser, *J. Raman Spectrosc.* **2009**, *40*, 499.
- [23] S. P. S. Porto, P. A. Fleury, T. C. Damen, *Phys. Rev.* **1967**, *154*, 522.
- [24] G. Turrell, in *Practical Raman spectroscopy* (Eds: D. J. Gardiner, P. R. Graves, H. J. Bowley, D. L. Gerrard, J. D. Loudon, G. Turrell (1st edn), Springer-Verlag: Berlin, **1989**, pp 13.
- [25] R. Loudon, *Adv. phys.* **1964**, *13*, 423.
- [26] U. Heinemeyer, R. Scholz, L. Gisslen, M. I. Alonso, J. O. Osso, M. Garriga, A. Hinderhofer, M. Kytka, S. Kowarik, A. Gerlach, F. Schreiber, *Phys. Rev. B* **2008**, *78*, 085210/1.
- [27] L. M. Ramaniah, M. Boero, *Phys. Rev. A* **2006**, *74*, 042505-1–042505-5.
- [28] R. Scholz, M. Schreiber, *Chem. Phys.* **2006**, *325*, 9.
- [29] D. A. Tenne, S. Park, T. U. Kampen, A. Das, R. Scholz, D. R. T. Zahn, *Phys. Rev. B* **2000**, *61*, 14564.
- [30] N. U. Zhanpeisov, S. Nishio, H. Fukumura, *Int. J. Quant. Chem.* **2005**, *105*, 368.
- [31] R. Scholz, A. Y. Kobitski, T. U. Kampen, M. Schreiber, D. R. T. Zahn, G. Jungnickel, M. Elstner, M. Sternberg, T. Frauenheim, *Phys. Rev. B* **2000**, *61*, 13659.
- [32] I. R. Lewis, L. Lewis, H. G. M. Edwards, *Handbook of Raman Spectroscopy: From the Research Laboratory to the Process Line*, CRC Press: New York, **2001**.
- [33] J. C. Decius, R. M. Hexter, *Molecular Vibrations in Crystals*, McGraw-Hill: New York, **1977**, p 391.
- [34] G. Salvan, *Metal/Organic/Inorganic Semiconductors Heterostructures Characterized by Vibrational Spectroscopies*, PhD thesis, Universität Chemnitz, **2003**.
- [35] A. Das, G. Salvan, T. U. Kampen, W. Hoyer, D. R. T. Zahn, *Appl. Surf. Sci.* **2003**, *212–213*, 433.
- [36] M. B. Casu, B.-E. Schuster, I. Biswas, H. Peisert, T. Chassé, *BESSY Annu. Rep.* **2007**, 177.
- [37] D. A. Long, *The Raman Effect: A Unified Treatment of the Theory of Raman Scattering by Molecules* (1 edn), John Wiley and Sons: Chichester, **2001**.
- [38] J. A. Woollam, B. Johs, C. M. Herzinger, J. Hilfiker, R. Synowicki, C. L. Bungay, *Crit. Rev. Opt. Sci. Technol.* **1999**, *CR72*, 3.
- [39] B. Johs, J. A. Woollam, C. M. Herzinger, J. Hilfiker, R. Synowicki, C. L. Bungay, *Crit. Rev. Opt. Sci. Technol.* **1999**, *CR72*, 29.